Article

Investigation of Applicability Flowdrill Technology for Joining Thin-Walled Metal Sheets

Anna Guzanová [1,*] **, Erik Janoško** [1] **, Dagmar Draganovská** [1] **, Marek Vrabeľ** [2] **, Miroslav Tomáš** [3] **, Peter Horňak** [4] **, Marek Vojtko** [5] **and Nikita Veligotskyi** [1]

1. Department of Technology, Materials and Computer Supported Production, Faculty of Mechanical Engineering, Technical University of Košice, Mäsiarska 74, 040 01 Košice, Slovakia; erik.janosko@tuke.sk (E.J.); dagmar.draganovska@tuke.sk (D.D.); nikita.veligotskyi@tuke.sk (N.V.)
2. Prototyping and Innovation Centre, Faculty of Mechanical Engineering, Technical University of Košice, Park Komenského 12a, 042 00 Košice, Slovakia; marek.vrabel@tuke.sk
3. Department of Automotive Production, Faculty of Mechanical Engineering, Technical University of Košice, Mäsiarska 74, 040 01 Košice, Slovakia; miroslav.tomas@tuke.sk
4. Institute of Materials and Quality Engineering, Faculty of Materials, Metallurgy and Recycling, Technical University of Košice, Letná 1/9, 042 00 Košice, Slovakia; peter.hornak@tuke.sk
5. Institute of Materials Research, Slovak Academy of Sciences, Watsonova 1935/47, 040 01 Košice, Slovakia; mvojtko@saske.sk
* Correspondence: anna.guzanova@tuke.sk

Abstract: The applicability of flowdrill technology to join steel and aluminum alloys is studied. When used to flowdrill two overlapped thin-walled materials, a joint is formed as a secondary effect. The quality of the resulting bushings forming the interference fit joint was investigated by metallography. The joints were formed using a combination of uncoated deep drawn steel, galvanized high-strength low alloy steel and aluminum alloy, in different positions in the joint. Subsequently, tensile shear testing of single joints was performed. The load-carrying capacity of the joints was also tested in combination with adhesive bonding. The combination of both technologies yields an increase in the dissipated energy of the joint at failure. The bonded connection provides a high maximum force at failure, the mechanical connection through bushings leads to an increase in the displacement value at failure, thereby increasing the area under the loading curve. The DC-Al joint showed the highest load-carrying capacity, up to 9 kN, as well as dissipative energy, up to 10.3 J. The joints were fractured by shearing of the inner bushing under tensile stress. The failure surfaces exhibited a typical ductile character with dimpled morphology. It was found that from the point of view of the load-carrying capacity of the joint, it is advisable to place a material with a higher melting temperature in the upper position in the joint. The combination of flowdrill technology with adhesive bonding results in a sealed joint with high load-bearing capacity, reduction in the risk of crevice and galvanic corrosion.

Keywords: flowdrill; adhesive bonding; joining; thin-walled sheet; dissimilar materials

1. Introduction

Joining dissimilar materials is one of the biggest challenges in the automotive and aerospace industries [1–5]. The challenge is to ensure a strong and safe joint of materials with different chemical compositions, different thicknesses, mechanical properties, formability, weldability, etc. Suitable technologies are various modifications of welding, bonding, and mechanical joining.

In fusion welding, the main problem is the mutual insolubility of certain elements, which limits the weldability of certain material pairs, in particular steels with aluminum alloys [6]. The most promising method is friction stir welding (FSW), where a forced mechanical mixing of the materials to be joined occurs without local melting. However, FSW technology is particularly suitable for joining more robust cross-sections [7,8].

Adhesive bonding technology has many well-known advantages—no weakening of the cross-section by drilling holes, uniform stress distribution, sealing of the joint, resistance of joints to galvanic and crevice corrosion, etc. The disadvantage lies mainly in the need for different preparation of the substrate surfaces [9,10].

The most promising technology for joining dissimilar materials is mechanical joining methods with or without a fastener [11]. The joining of materials occurs as a result of controlled plastic deformation, pressure at the contact interface of the parts, and their mutual wedging. There is no thermal influence on the materials to be joined, different thicknesses of the materials to be joined can be combined without pre-treatment of the surfaces and without risk of damage to any protective surface layer, and in a very short time (a few seconds). Mechanical joining methods such as clinching, self-piercing riveting, and their myriad variations or combinations with bonding or resistance welding are well-known and relatively well studied [12,13]. The limiting factor of the above-mentioned mechanical joining methods is the lower load-bearing capacity of mechanical joints compared to spot-welded joints, the risk of mutual rotation of the materials to be joined, the difficult repair of incorrectly made mechanical joints, the low level of standardization, and above all the necessity of two-sided access to the materials to be joined, which prevents their use on hollow extruded or hydroformed profiles.

Joining with flow drilling screws, on the other hand, requires the creation of a hole on one of the materials, the other is drilled with a flowdrill tool, which is simultaneously a screw. However, the weight of the resulting joint is still increased by the weight of the joining element [14–28].

Therefore, the mention of Schmerler et al. in [29] about the possibility of using flowdrill technology for joining two or three materials without using a screw, just by forming a bushing, attracted the attention of the authors of this paper. A kind of bushing is formed in the material heated by the friction heat, which can be used to form a thread. The authors [29] used flowdrill technology to form an Al-fiber-reinforced polymer-Al joint, whereby the heat of drilling softens the polymer matrix and the tool penetrates it without disrupting the continuity of the fibers. Schmerler [29] also mentioned the possibility of this method working with other combinations of blanks, such as aluminum/steel/aluminum.

Confirming the possibility of joining two or three materials only by thermal drilling without a screw, this method would bring the advantages of joining materials with a one-sided approach, a chipless joining method, elimination of the need to pre-drill holes, higher precision of the position of the parts, the possibility of creating sandwich structures of metal-composite-metals from different materials. The principle could find application in mechanical engineering, automotive industry, rail vehicle, and ship manufacturing, as well as aerospace engineering. The work of [29] is a unique paper dealing with this possibility of joining and was the main motivation of the authors of the paper in designing the experimental concept.

In flowdrill process, the frictional heat (600–800 °C) softens the material and makes it easier for the tool to penetrate the material [1–5,11]. As the tool penetrates, there is a plastic flow of material in the direction of the tool feed, which creates bushing, as well as against the direction of tool movement, which creates a collar [14]. According to Shalamov et al. [15], depending on the thickness of the bonded material, the proportion of material involved in bushing formation also varies. They found that thin materials use up to 100% of the deformed volume for bushing formation (collar formation is suppressed), and with increasing material thickness, this proportion is smaller. The quality and integrity of the bushing are extremely important for the strength of the joint and are affected by the properties of the material joined (thermal conductivity, plasticity, formability), as well as by process parameters [16,18–30].

Özek et al. [19], dealt with thermal drilling of various aluminum alloys at different speeds and feeds. They found that high spindle speeds and feed rates in thermal drilling of low thermal conductivity aluminum alloys lead to high frictional heat, which is reflected in the

quality of the bushing formed. The quality and compactness of bushing can also be controlled by external influences, e.g., by introducing pure argon gas into the flowdrill process [20].

When using flowdrill technology to join two thin-walled materials, the gap that arises between the materials due to their different formability under axial force and due to the bushing formed on the top material pushing out the bottom material [31] can appear to be a problem. The gap is smaller when using a connecting screw, which presses both materials together when tightening. When combining flowdrill technology with adhesive bonding, the adhesive could fill the gap and thus prevent possible crevice corrosion.

The aim of the experimental work was to verify the possibility of using flowdrill technology for joining thin steel and aluminum sheets. At the same time, the possibility of combining thermal drilling with adhesive bonding was tested.

2. Materials and Methods

2.1. Materials of Workpieces

The following materials were used for joints preparation:

- Cold rolled uncoated deep drawing steel DC04, used for the production of interior and exterior parts of car bodies and for other stampings.
- Zinc-galvanized fine-grained high-strength microalloyed steel TL 1550-220+Z with increased cold formability.
- Precipitation hardened aluminum alloy EN AW-6082 T6 (AlSi1MgMn).

The chemical composition of materials, their mechanical and physical properties and surface conditions are given in Tables 1–3.

Table 1. Chemical composition of the materials, wt. %.

DC04									
C	Mn	P	S	Fe	-	-	-	-	-
0.040	0.250	0.009	0.008	bal.	-	-	-	-	-
TL 1550-220+Z									
C	Mn	Si	P	S	Al	Nb	Ti	Cu	Fe
0.100	1.000	0.500	0.080	0.030	0.015	0.100	0.150	0.200	bal.
EN AW-6082 T6									
Si	Fe	Cu	Mn	Mg	Cr	Zn	Ti	Al	-
1.00	0.40	0.06	0.44	0.70	0.02	0.08	0.03	bal.	-

Table 2. Mechanical properties and some specific conditions of the materials.
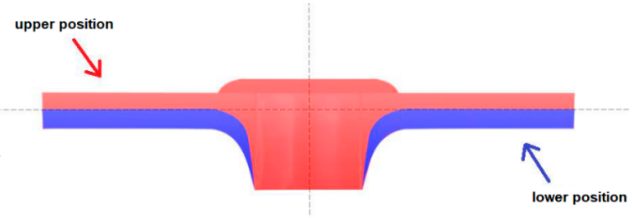
Materials	YS (MPa)	UTS (MPa)	Elongation (%)	Thickness (mm)	Condition
DC04	197	327	39	0.8	electrostatically oiled
TL 1550-220+Z	292	373	34	0.8	Zn coated, 100 g·m^{-2}
EN AW-6082 T6	290	340	14	1.0	solution treated, artificially aged

Table 3. Physical properties of the materials.

Material	Density (kg·m^{-3})	Melting Point (°C)	Therm. Conductivity (W·m^{-1}·K^{-1})	CTE (10^{-6}·K^{-1})	Modulus of Elasticity (GPa)
DC04, TL 1550-220+Z	7860	~1500	45	10.8–12.5	~210
EN AW-6082 T6	2700	555	180	24	~70

Joints were created between two dissimilar materials, while the position of materials in the joint was alternated, but for comparison, joints of the same materials were also created. Table 4 shows a complete matrix of all material combinations in joints.

Table 4. Matrix of created joints.

Scheme of Positioning Materials in the Joint	Material in Upper Position	Material in Lower Position
	DC	DC
		TL
		Al
	TL	DC
		TL
		Al
	Al	DC
		TL
		Al

2.2. Flowdrill Tool, Parameters of the Drilling Process

According to the thickness of the materials to be joined and the thickness of the overall joint, the Flowdrill Long ø 5.3 mm thermal drilling tool (Flowdrill Inc., Arnold, MO, USA) was selected. The process parameters are shown in Table 5.

Table 5. Parameters of the drilling process.

Tool Appearance	Variable	Value
	Rotation speed	7200 rpm
	Tool feed rate	200 mm/min
	dwell time in lowest reversal position	0.8 s

To prevent the two materials from being pushed apart during bushing formation and creating a gap between them, the tool entered the material up to 0.1 mm below the surface level of the upper material and remained there for 0.8 s, Figure 1. This pressed the materials together while they were firmly supported (embedded in the jig) from the underside. This work cycle was carried out on a DMC 635V ecoline milling center (DMG Mori Aktiengesellschaft, Bielefeld, Germany).
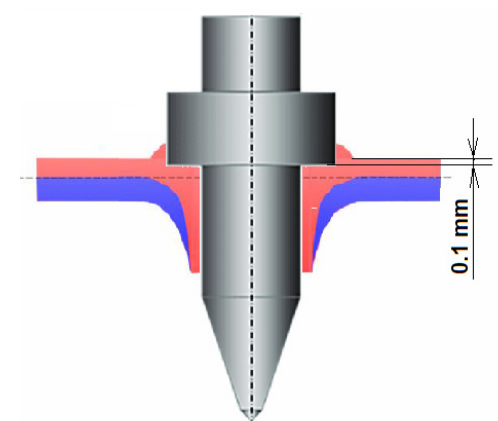
Figure 1. Tool in the lowest reversal position.

2.3. Shape and Dimensions of Test Specimens

When calculating the dimensions of the test specimens, we followed EN ISO 12996 [32], according to which the dimensions of the test specimens are based on the diameter of the mechanical joining member, in our case the diameter of the hole-making tool and the

bushings in the materials to be joined. The resulting dimensions of the test specimens are shown in Figure 2. The hole is always formed in the center of the overlapped area.
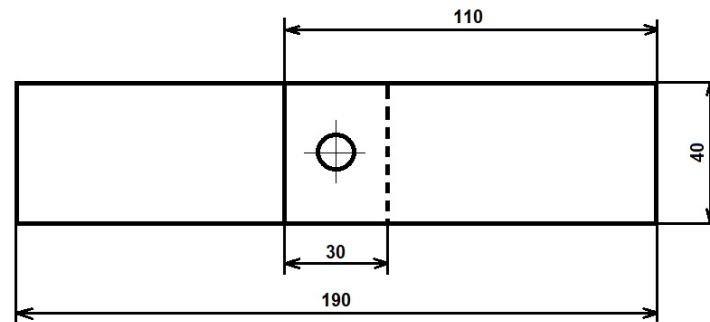

Figure 2. Shape and dimensions of joint assembly in mm.

2.4. Adhesive and Adhesive Bonding Process

Once the holes were drilled and the joints formed, it was found that not all material pairs would form a bushing of sufficient height to carry the load. Those material combinations were excluded from further experiments and the combination of adhesive bonding and thermal drilling was further tested only for joints with a sufficiently large bushing. RB 5197 adhesive (Henkel AG & Co. KGaA, Düsseldorf, Germany), which is rubber-based and suitable for combination with resistance welding, was used to bond the specimens. The thickness of the adhesive was 0.2 mm. The preparation of the bonded materials prior to bonding consisted of degreasing and immersion in an organosilane agent to improve adhesion of the adhesive. The procedure for the formation of the combined joints is as follows: degreasing, application of organosilane, application of adhesive, overlapping of materials, thermal drilling, curing of the adhesive at 175 °C, 25 min in the oven. Tensile strength of the adhesive is 12 MPa, shear strength at 20 °C is >15 MPa.

2.5. Testing of Joint Assemblies

The prepared joints were tested for shear strength under tensile stress on a TIRA test 2300 universal testing machine (TIRA GmbH, Schalkau, Germany) at a loading rate of 10 mm·min^{-1}. The load-displacement dependence was recorded during loading. From the obtained dependencies we determined selected following mechanical characteristics of the joints, recommended by EN ISO 12996:

Fmax—tensile shear force, the maximum force recorded during the test.
s_{Fmax}—displacement at the tensile shear force Fmax.
0.3Fmax—tensile shear force on the downward part of the curve corresponding to 30% of Fmax.
s0.3Fmax—displacement at 0.3Fmax.

The 0.3Fmax characteristic arose from the need to express the energy of the joint dissipated during the test as the area under the loading curve. In an attempt to reduce the test time, the 0.3Fmax characteristic was introduced at which the test may terminate, as generally the area under the curve beyond 0.3Fmax is small and does not contribute significantly to dissipated energy.

3. Results

3.1. Visual Assessment of Joints

When joining selected material pairs, it is expected that by heating and forming the materials, bushing will occur in addition to hole formation. The material in the top position forms the inner bushing in the joint, the bottom material forms the outer bushing in the joint. When thermally drilling the materials, some material combinations were able to form a solid joint that resisted moderate effort to separate the materials, but some pairs failed to form a solid joint.

The appearance of the formed joints is shown in Table 6.

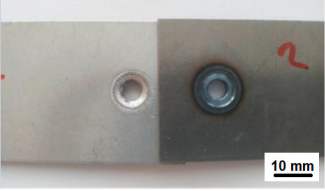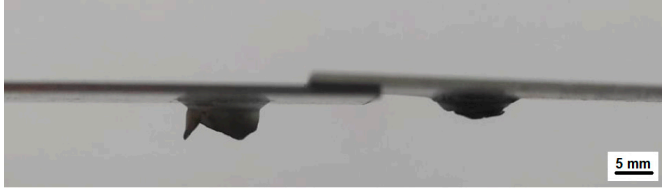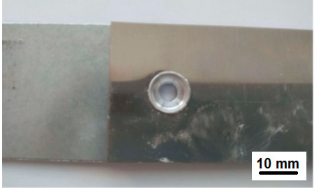**Table 6.** Appearance of the created joints (top and front view).
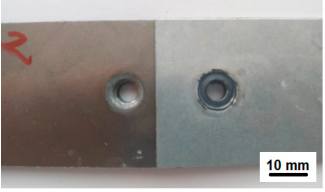
Mat. in Upper Position	Mat. in Lower Position	Top View	Front View
DC	DC		
DC	TL		
DC	Al		
TL	DC		
TL	TL		
TL	Al		
Al	DC		

Table 6. *Cont.*

Mat. in Upper Position	Mat. in Lower Position	Top View	Front View
Al	TL		
Al	Al		

According to [9–11], the quality of the joints is related to the shape and integrity of the bushings formed from both materials. It is desirable that a solid compact bushing is formed. A disturbed bushing (cracks, petals) is undesirable as it cannot be threaded–which is the primary objective of thermal drilling (flowtapping), and when joining, a disturbed outer bushing does not form a fit joint with the inner bushing, which is the objective of joining.

Among the joints formed, an intact outer bushing can be observed in DC-DC, TL-DC, Al-DC, Al-TL, and Al-Al joints. For the DC-DC and TL-DC joints, despite the solid outer bushing, no connection was formed because no inner bushing was developed in the top material. The materials therefore separated after release from the fixture. Only the Al-DC, Al-TL, and Al-Al pairs formed a solid joint.

Surprisingly, on the other hand, a joint was formed in the TL-Al material pair where petals were observed on the outer Al bushing. For the DC-TL joint, the upper DC material did not form an inner bushing of sufficient height and the outer bushing of the lower TL material was broken. When the joint was loaded, the pieces separated. For the DC-Al joint, the top material DC formed a continuous inner bushing of sufficient height, but the outer bushing of the bottom material Al exhibited petals. For the TL-TL joint, continuous but relatively short bushings were formed, so there was no joint formation.

3.2. Macroscopic Evaluation of Joints

Table 7 shows macroscopic sections through individual joints to better see the shape of the outer and inner bushings. The materials of the failed joints were additionally bonded together with adhesive (black in color) so that they could be cut and embedded in resin.

It is clear from the metallographic sections that the outer bushing was always successfully formed during thermal drilling, but in some (the aforementioned) cases it was not continuous. The only case where two parallel bushings of the relevant height were formed was the DC-Al joint. For the other joints that reached the handling resistance, the connection between the materials was apparently formed on a different basis, e.g., due to friction between the materials during plastic deformation at elevated temperature during thermal drilling. The material combinations of the successfully formed joints were subsequently used to produce joints combined with adhesive bonding. Metallographic sections of the combined joints are shown in Table 8.

The metallographic sections show an intact outer bushing at almost all joints, the bushing at the Tl-Al joint is slightly distorted. Parallel bushings of the both joined materials were formed only at the DC-Al and TL-Al joints. The other joints that have reached the handling strength and have not formed an inner bushing are apparently friction joints, not forming fit joints.

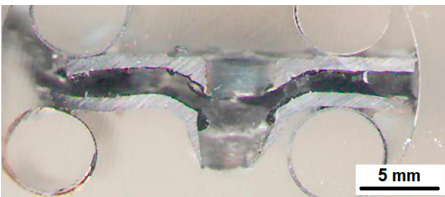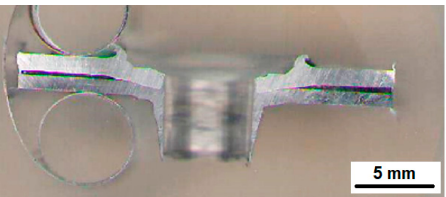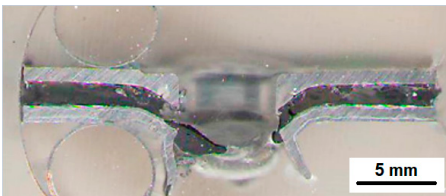**Table 7.** Macroscopic sections of individual flowdrill joints.
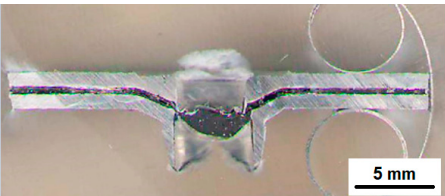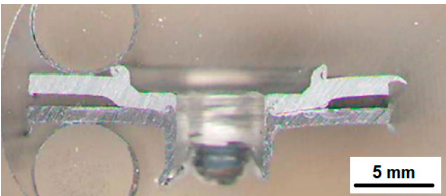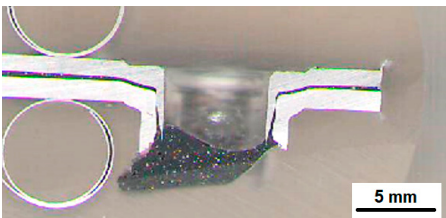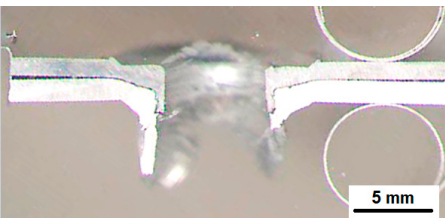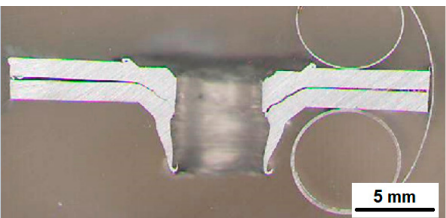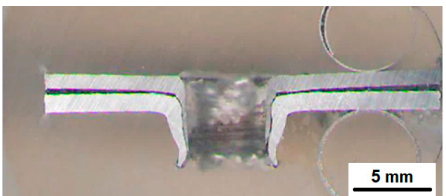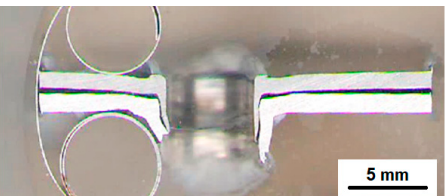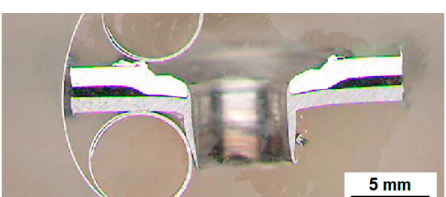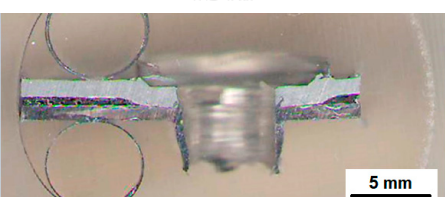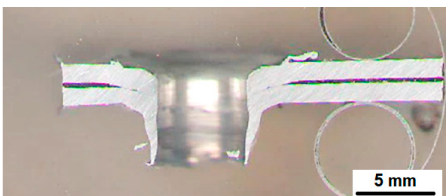
DC in Upper Position	TL in Upper Position	Al in Upper Position
5 mm DC-DC	5 mm TL-DC	5 mm Al-DC
5 mm DC-TL	5 mm TL-TL	5 mm Al-TL
5 mm DC-Al	5 mm TL-Al	5 mm Al-Al

Table 8. Macroscopic sections of individual combined joints.

Successfully Formed Joints with Al in Upper or Lower Position	
5 mm DC-Al	5 mm TL-Al
5 mm Al-DC	5 mm Al-TL
5 mm Al-Al	

3.3. Microscopic Evaluation of Joints

From Table 8 it can be seen that successful joints were formed when one of the materials was an Al alloy. Metallographic cross sections of the successfully formed joints, where at least one material is Al alloy, taken at 50× magnification, are shown in Figures 3–5.
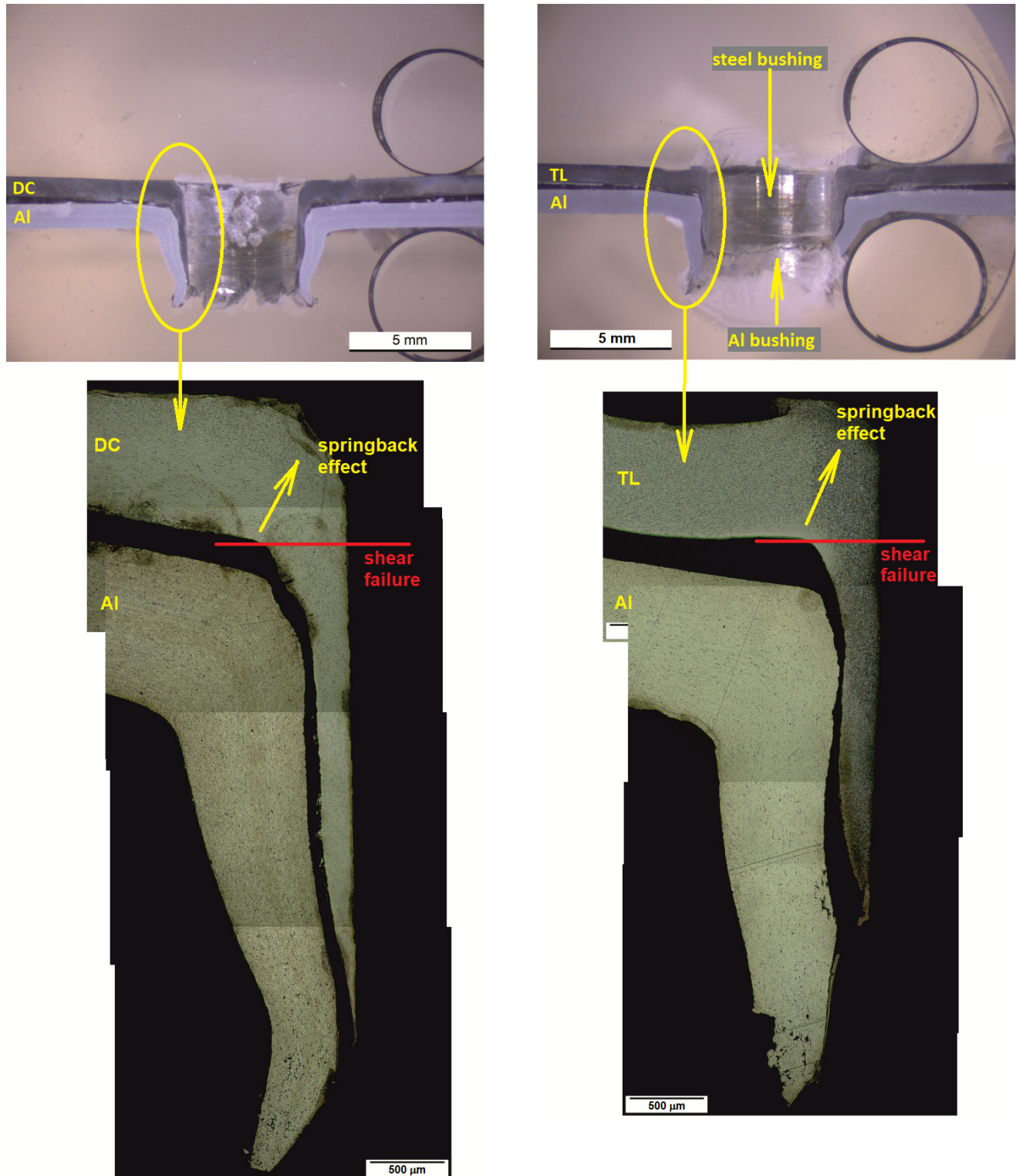
Figure 3. Cross sections of DC-Al and TL-Al joints, etched: Nital, HF.
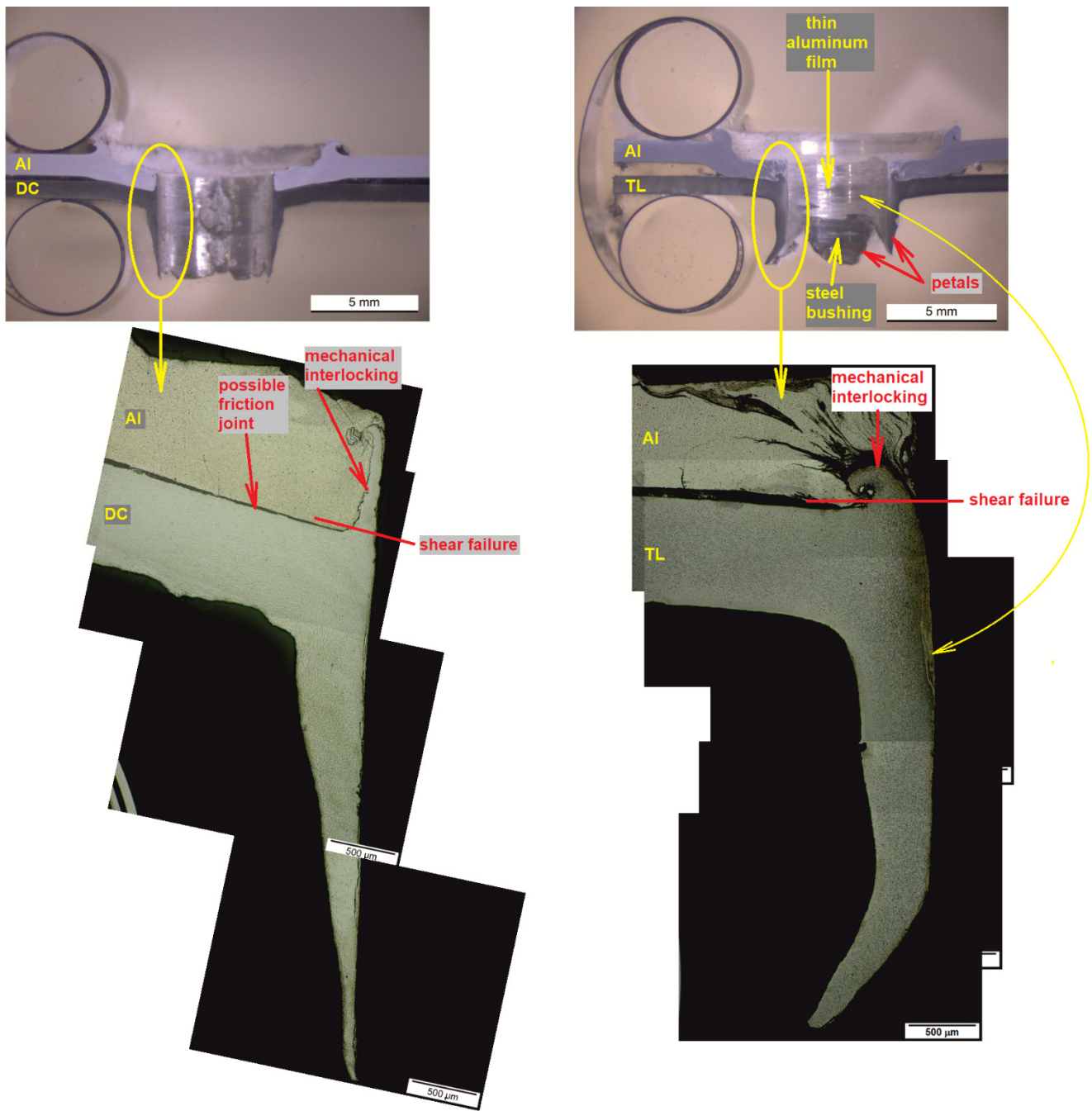
Figure 4. Cross sections of Al-DC and Al-TL joints, etched: Nital, HF.

Figure 3 shows the metallography of the joints, where steel materials are in the upper position and Al in the lower position. For both joints, it can be seen that both the resulting bushings (steel and aluminum) underwent the forming process simultaneously, as evidenced by the identical transverse profile of both bushings. After the tool left the materials, the vertical clamping force from the flange part of the tool ceased and the steel was sprung back, creating a gap between the inner and outer bushing. The red line indicates the location where shear failure of the bushing will occur under load.

Figure 4 shows the metallography of the joints, where the steel materials are in the lower position and the Al alloy in the upper position.
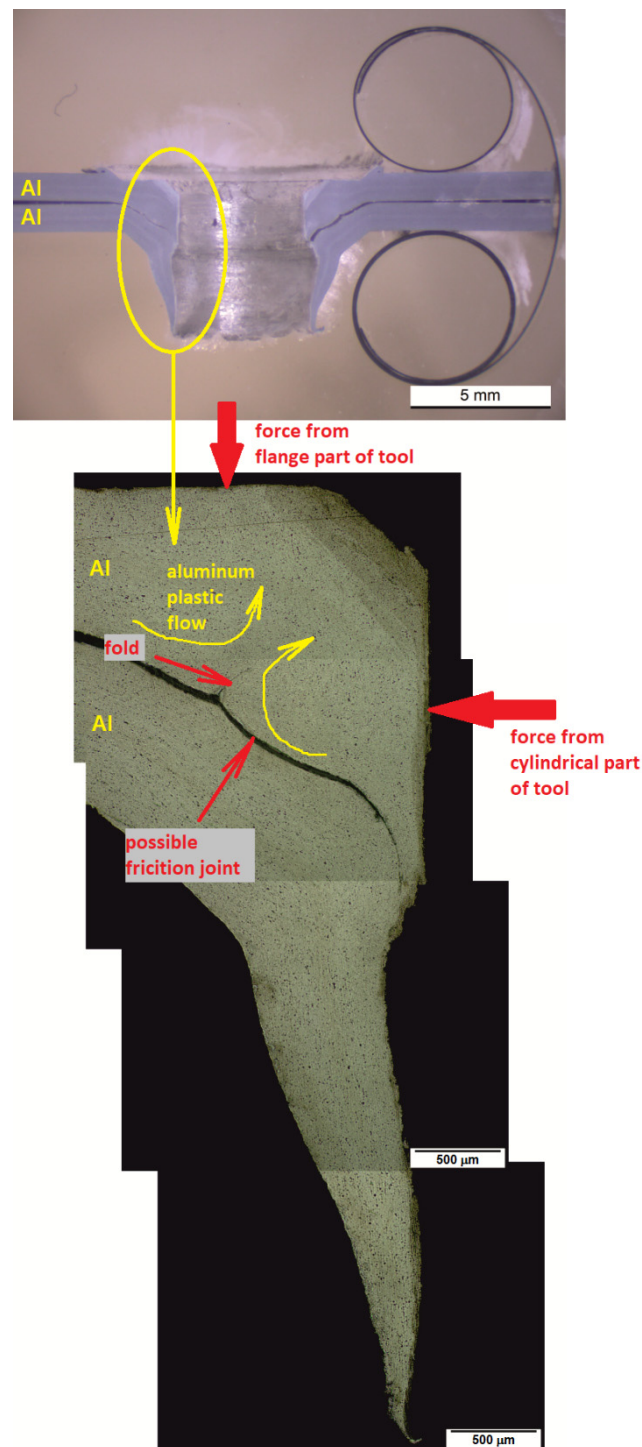
Figure 5. Cross section of Al-Al joint, etched: HF.

Cross sections on Figure 4 reveal details that were not observable by the naked eye. In both joints (Al-DC and Al-TL), only one bushing was formed—the steel bushing. The aluminum alloy in the upper position was pushed out from the hole location sideways. The steel in the upper position exhibited plastic flow both in the direction of tool feed as well as against the direction of tool feed. The plastic flow of the steel in the direction of the tool feed created the bushing. A smaller volume of material was also displaced against the direction of tool feed and formed a barrier between the aluminum alloy and the tool. This small protrusion would create a collar when drilling one material. Now, however, it wedged into the aluminum alloy and formed a mechanical interlocking joint with it. In the

Al-TL joint, a very thin film of aluminum alloy is spread on the inner surface of the steel bushing locally. For DC material, the collar is higher than that of TL ste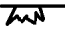el, which is related to the lower mechanical properties and higher ductility of DC steel compared to TL. The metallography of the above joints shows that failure of this type of joint will be realized by shear of the collar and failure of the likely friction joint at the horizontal interface of the materials.

Figure 5 shows the metallography cross section of the Al-Al joint.

From Figure 5, it can be seen that the Al in the upper position was pushed out laterally by the cylindrical part of the tool and at the same time it was pushed from the top by the flanged part of the tool, which caused the thickness increase of the Al sheet in the upper position near the hole above the original thickness. The plastic flow of the Al alloy is indicated by the yellow arrows in Figure 5. The consequence of the indicated plastic flow is the formation of a fold on the bottom surface of the upper sheet. During the intense plastic flow of the upper material, suitable conditions for the formation of a potential frictional joint between the materials were created. The contact area of the two materials in the vicinity of the hole is strongly conical and the resulting joint is thus partly frictional and partly form-fitting.

The findings are summarized in Table 9.

Table 9. Basic characteristics of the joints produced.

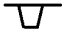| Material Combination	Bushing	Max. Bushing Wall Thickness (mm)	Bushing Height (mm)	Compactness of Bushing	Type of Joint	Handling Resistance
DC-DC	inner (DC)	-	1.6	short bushing	-	no
	outer (DC)	0.6	3.6	long compact bushing		
DC-TL	inner (DC)	-	1.4	short bushing	-	no
	outer (TL)	0.6	3.4	bushing with petals		
DC-Al	inner (DC)	0.4	3	long compact bushing	interference fit joint	no
	outer (Al)	0.8	2.5	bushing with petals		
TL-DC	inner (TL)	-	1.4	short bushing	-	no
	outer (DC)	0.6	3.4	long compact bushing		
TL-TL	inner (TL)	-	0.8	short bushing	-	no
	outer (TL)	0.6	3.4	long bushing with little cracks		
TL-Al	inner (TL)	0.35	1.3	short bushing	interference fit joint	yes
	outer (Al)	0.75	3.3	bushing with petals		
Al-DC	inner (Al)	-	0.6	-	Mechanical interlocking/friction joint	yes
	outer (DC)	0.6	3.6	long compact bushing		
Al-TL	inner (Al)	-	-	-	Mechanical interlocking/friction joint	yes
	outer (TL)	0.6	3.4	long bushing with little cracks		
Al-Al	inner (Al)	-	1.6	short bushing	friction joint/interference fit joint	yes
	outer (Al)	0.8	3.8	long compact bushing		

—long compact bushing   —long bushing with little cracks   —short bushing   —bushing with petals.

Appearance of the fracture surfaces of the TL-Al joint are shown in Figure 6. The fracture surfaces of the other joints looked similar.

In Figure 6a, the arrow points to the area of shear failure of the bushing. In Figure 6b, the arrow points to the shear-separated bushing at the joint failure. It can also be seen from Figure 6b that during thermal drilling, the uncured adhesive was pushed out from the vicinity of the hole. The bonded joint failure was cohesive for all tested joints.

(**a**)   (**b**)
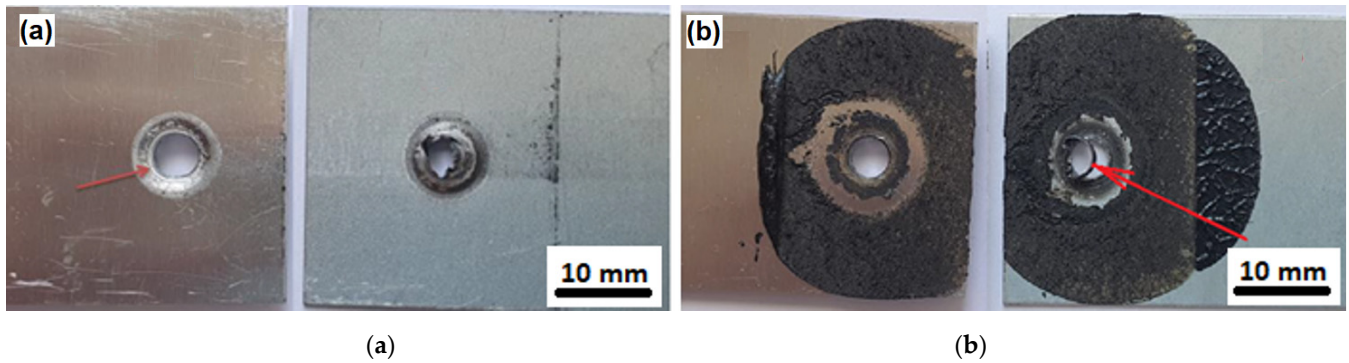
Figure 6. Fracture surface of TL-Al joint made by (**a**) FD, (**b**) FD + AB technology.

3.4. SEM Analysis of Joints

SEM analysis of individual joints are shown in Figures 7–11.
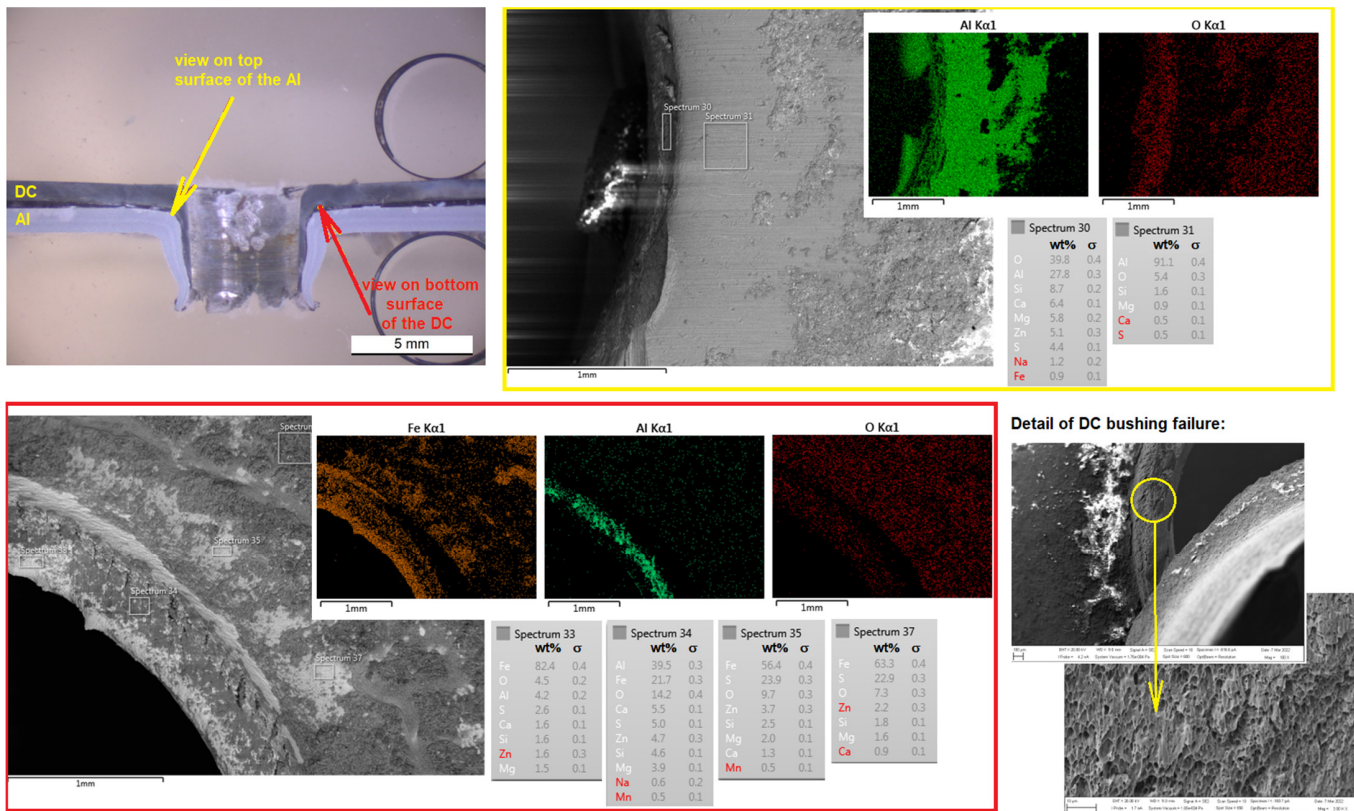
Figure 7. SEM analysis of DC-Al joint, element maps, EDS spectra, and fracture surfaces of bushing. The yellow border contains a detailed view on the top surface of the lower material. The red border contains a detailed view on the bottom surface of the upper material.
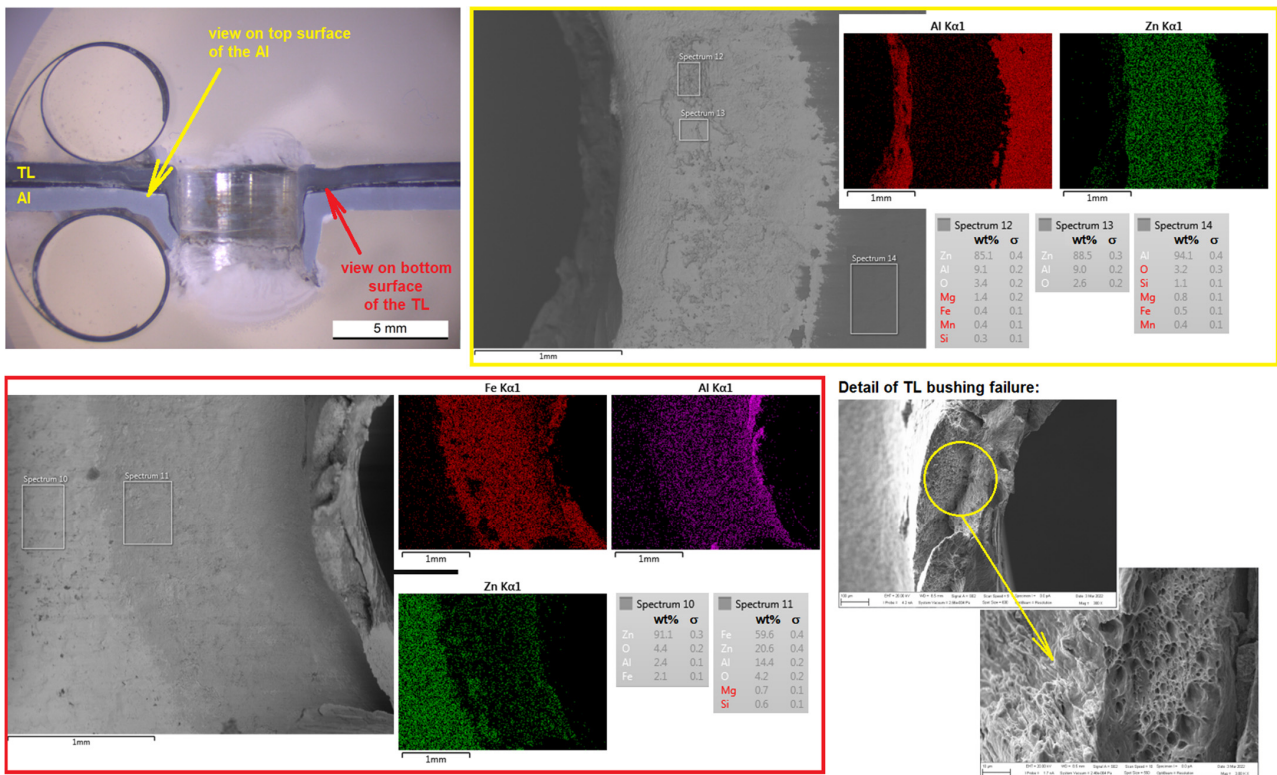
Figure 8. SEM analysis of TL-Al joint, element maps, EDS spectra and fracture surfaces of bushing. The yellow border contains a detailed view on the top surface of the lower material. The red border contains a detailed view on the bottom surface of the upper material.
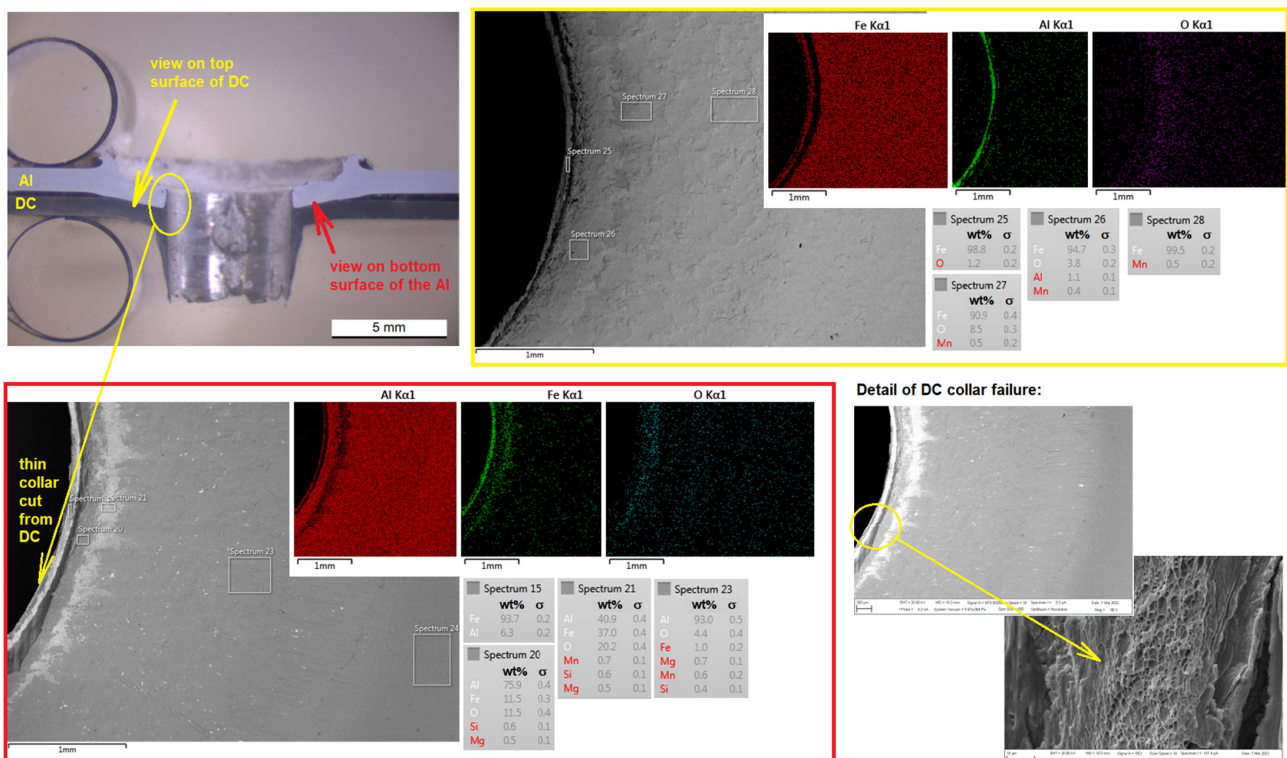
Figure 9. SEM analysis of Al-DC joint, element maps, EDS spectra, and fracture surfaces of bushing. The yellow border contains a detailed view on the top surface of the lower material. The red border contains a detailed view on the bottom surface of the upper material.
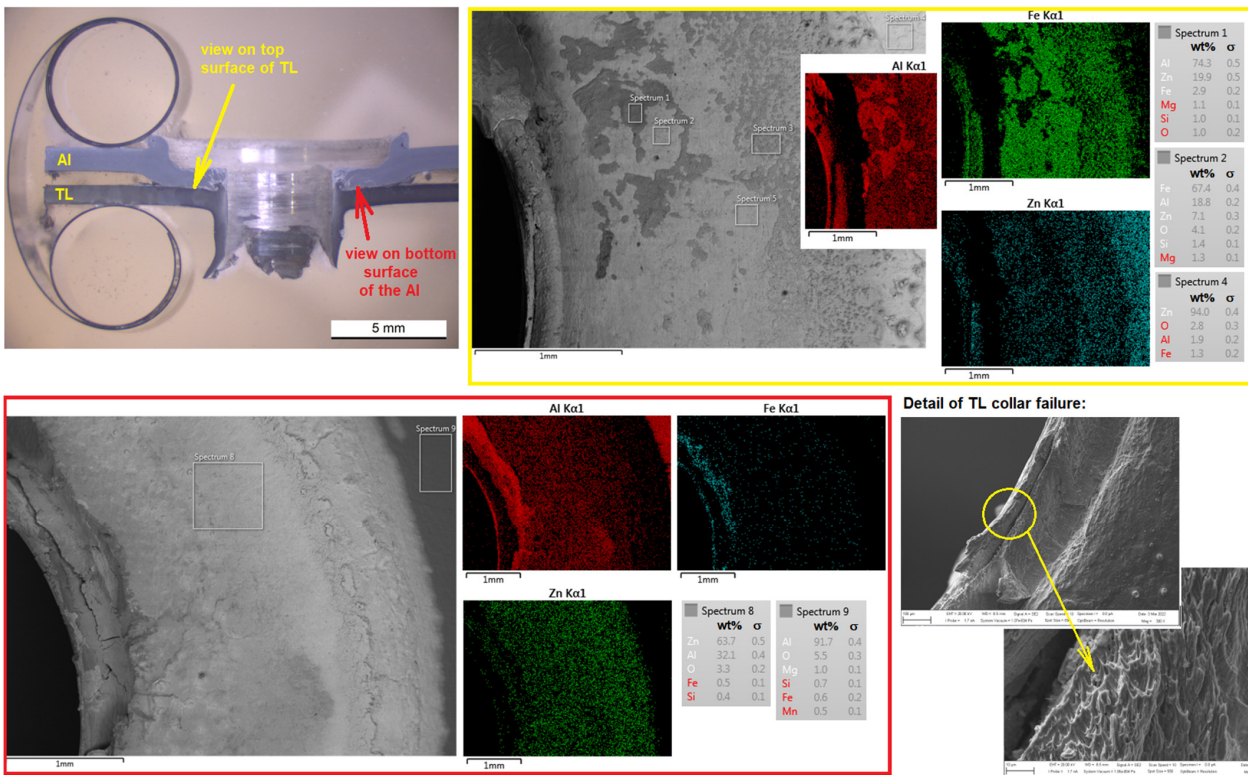
Figure 10. SEM analysis of Al-TL joint, element maps, EDS spectra, and fracture surfaces of bushing. The yellow border contains a detailed view on the top surface of the lower material. The red border contains a detailed view on the bottom surface of the upper material.
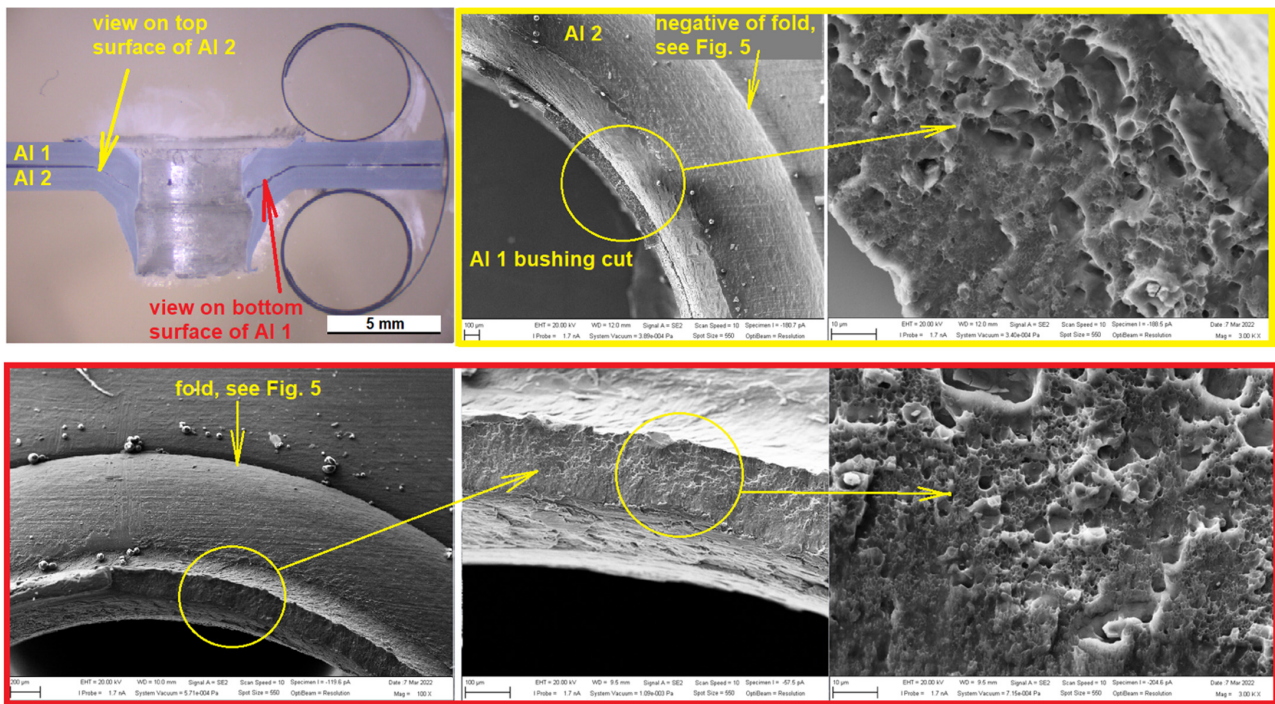
Figure 11. SEM analysis of Al-Al joint, element maps, EDS spectra, and fracture surfaces of bushing. The yellow border contains a detailed view on the top surface of the lower material. The red border contains a detailed view on the bottom surface of the upper material.

Figure 7 proved, that the contact surface of the Al alloy does not show the presence of DC-derived elements, as confirmed by maps and spectra from the area. The presence of O is indicative of oxidation of both surfaces, which occurred due to heating during drilling. The DC contact surface locally contains Al, which was transferred during shear failure of the bushing. Detail of the DC bushing failure confirms a typical ductile fracture with a dimple morphology. The dimples show deformation in the direction of the applied shear stress when the joint is tested.

The contact surface of the Al alloy shows an adhesively bonded layer of Zn from the TL material near the hole, as confirmed by maps and spectra from the area, Figure 8. The TL contact surface near the hole reciprocally contains a minor amount of Al that was transferred by friction of the materials during drilling. Detail of the TL bushing failure confirms again a typical ductile fracture with a dimpled morphology oriented in the stress direction.

Figure 9 shows that the contact surface of the DC steel exhibits minimal presence of Al in the vicinity of the hole. Both surfaces contain O indicative of oxidation processes during drilling. The Al contact surface in the vicinity of the hole reciprocally contains a minimal amount of Fe deposited adhesively from the counter material. Detail of the DC collar failure confirms again a typical ductile fracture with dimpled morphology.

The contact surface of the TL shows an adhesively deposited layer of Al in the form of discontinuous islands in the vicinity of the hole, as confirmed by maps and spectra from the area, Figure 10. The Al contact surface in the vicinity of the hole contains a relatively continuous layer of adhesively deposited Zn from the TL material. Detail of the TL collar failure confirms again a typical ductile fracture with dimpled morphology oriented in the strain direction.

The Al-Al joint, Figure 11, is the only joint among the other analyzed joints in which the Al bushing failed. The fracture surface of the Al bushing in the top position exhibits, like steel, a ductile fracture with dimpled morphology. The fold that can be observed in the metallographic section of the joint, Figure 5, is also visible in the SEM images.

A comparison of the appearance of the surface morphology of the original Al sheet and the surface of the Al sheet near the joint is shown in Figure 12. The surface near the joint shows signs of directional deformation, intense friction, partial melting, and an overall change in the original morphology compared to the original surface.
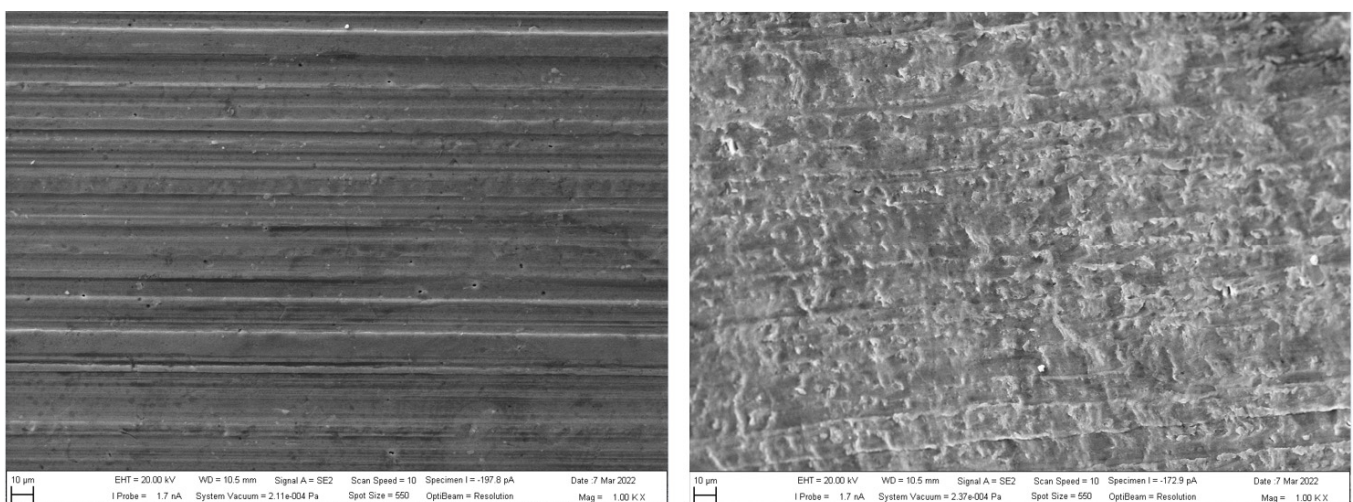
Figure 12. Comparison of original surface of Al sheet (**left**) and contact surface near joint (**right**), SEM.

3.5. Testing of Joints

The formed joints, which were manipulable, were then subjected to a tensile shear strength test. From the schematic diagram of the formed joints (Figure 13a), it can be seen that the load-carrying capacity of shaped joints having two concentric bushings will depend on the properties and thickness of the inner bushing formed from the material in

the upper position. This is because when the joint is subjected to tensile stress, the inner bushing will be damaged by shear. The outer sleeve has only a supporting function in the joint and remains intact after the test.

(**a**)   (**b**)
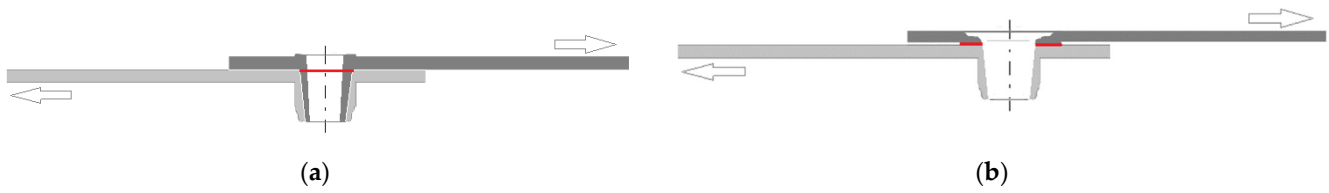
Figure 13. (**a**) Schematic diagram of the failure of a fit joint by shearing of the inner bushing, (**b**) Schematic diagram of friction joint failure. The shear plane is marked in red. The arrows indicate the direction of the load.

For joints where only the outer bushing and thin collar of the bottom material has been formed, the load-carrying capacity of the joint will depend on the width and quality of the frictional bond of the materials around the hole and the collar thickness, Figure 13b. Load–displacement curves of individual connections are shown in Figure 14.
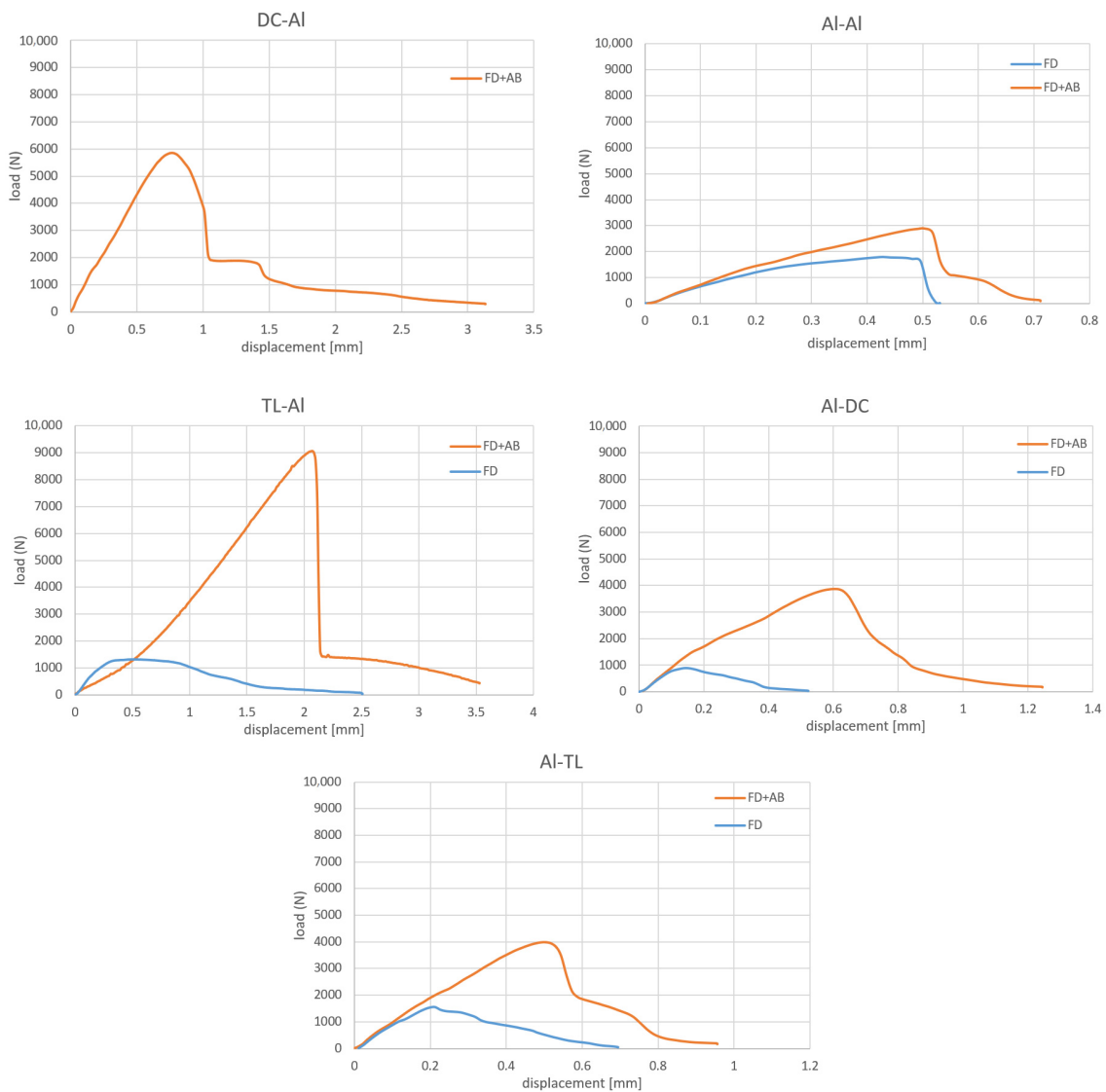
Figure 14. Comparison of loading curves of flowdrill joints (FD) and joints combined with adhesive bonding (FD + AB).

From the load-displacement curves of the joints formed only by FD technology, it is clear that the joints where the Al material was in the upper position always failed at displacement values up to 1 mm, while the Tl-Al joint failed at higher displacement values-up to 2.5 mm. This indicates a higher ability of the Tl-Al joint to dissipate energy under stress. For all FD joints, the descending part of the curve is gradual, it is not an instantaneous drop in force, but gradual shearing of the bushing occurs.

The loading curves of FD + AB connections show a significantly higher maximum force compared to FD connections. Two regions are evident on the downward part of the curve: the drop from the maximum force is steep, indicating adhesive failure, then there is a gradual descent, corresponding to gradual failure of the bushing and occurring at approximately the Fmax level of the corresponding FD joint, Figure 15.
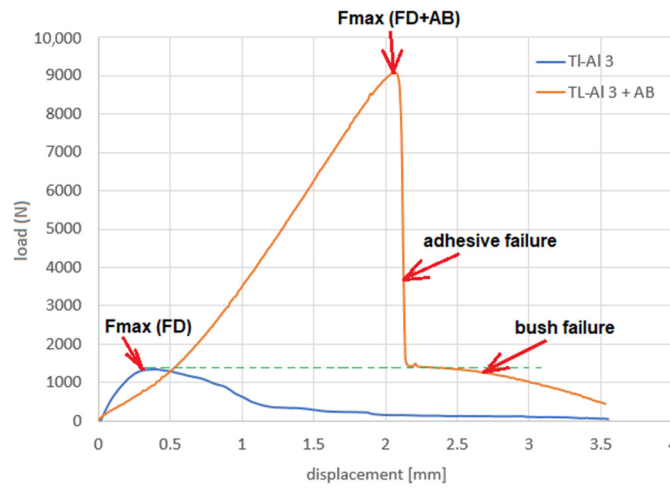
Figure 15. Typical regions on load-displacement curves.

A comparison of typical load-displacement curves of all flowdrill joints and joints combined with adhesive bonding are shown in Figure 16.

(a)   **(b)**
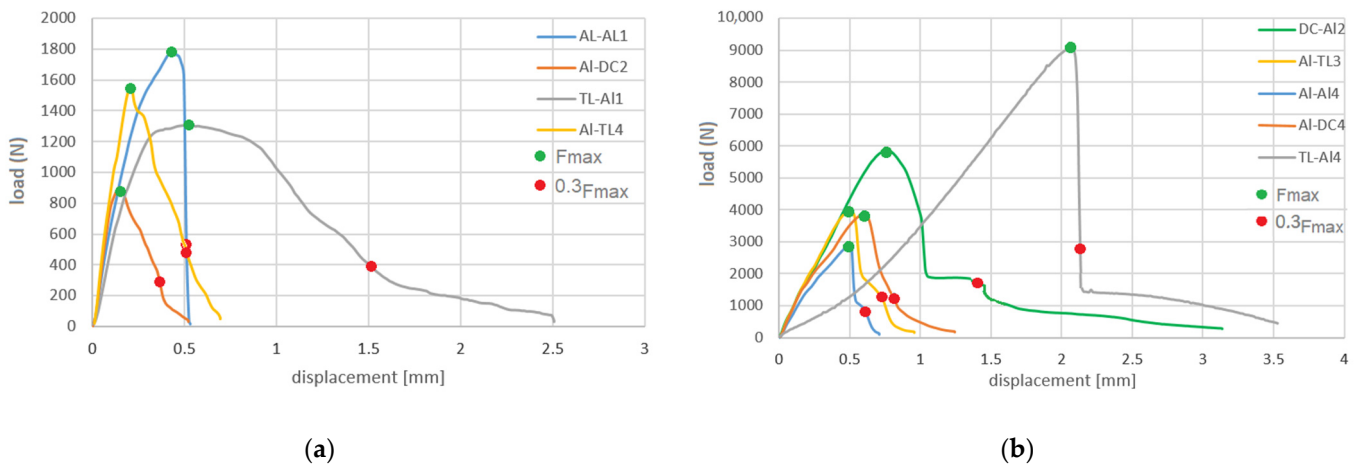
Figure 16. Load–displacement curves successfully made by (**a**) FD and (**b**) FD + AB technology.

From Figure 16, it can be seen that joints combined with adhesive bonding have several times higher load-carrying capacity than FD joints. The contribution of FD to the overall load capacity of the joint is to slow down the downward part of the curve and to increase the overall energy dissipation of the joint by the shear of the bushing. From this perspective, it is therefore important to produce a compact bushing with the greatest possible thickness in the shear plane.

The area under the load-displacement curve represents the energy required to fracture the joint, or dissipated energy up to fracture. The dissipated energy up to fracture, assuming a linear increase in force, can be approximately calculated according to Equation (1):

$$W = (F_{max} \times s_{Fmax})/2 \tag{1}$$

The area under the load–displacement curve was calculated by the trapezoidal method by approximating the area under the curve using the Riemann integral:

$$W = \int_0^{s\ max} F(s)ds \approx \sum_{i=1}^{n} F_i(\overline{s_i})\Delta s = \Delta s[F_1(\overline{s_1}) + F_2(\overline{s_2}) + \cdots + F_n(\overline{s_n})] \tag{2}$$

where $\Delta s = s_i - s_{i-1}$, $\overline{s_i}$ is the midpoint of the displacement interval $[s_{i-1}, s_i]$ and $F_i = (F_i + F_{i-1})/2$.

A comparison of the dissipated energy values for the particular material combinations and joining methods is given in Table 10.

Table 10. Basic characteristics of joints and dissipated energy up to fracture.

Combination	Fmax (N)	s_{Fmax} (mm)	0.3Fmax (N)	s0.3Fmax (mm)	W * (Fmax) (J)	W ** (Fmax) (J)	W *** (J)
Joining by Flowdrill							
DC-Al	-	-	-	-	-	-	-
Al-DC	834	0.15	250	0.35	0.06	0.08	0.23
TL-Al	1300	0.40	390	1.12	0.26	0.47	1.61
Al-TL	1569	0.24	471	0.49	0.19	0.21	0.53
Al-Al	1770	0.44	531	0.54	0.39	0.48	0.62
Joining by Flowdrill + Adhesive Bonding							
DC-Al	5857	0.77	1757	1.40	2.25	2.49	5.70
Al-DC	3861	0.60	1158	0.80	1.16	1.35	2.07
TL-Al	9077	2.07	2723	2.13	9.39	8.32	10.31
Al-TL	3993	0.51	1198	0.74	1.02	1.14	1.72
Al-Al	2890	0.50	867	0.60	0.72	0.82	1.01

* Dissipated energy up to Fmax according to Equation (1). ** Dissipated energy up to Fmax according to Equation (2). *** Total dissipated energy up to fracture according to Equation (2).

From the point of view of dissipated energy under load, it is advantageous when the above characteristics reach the highest possible values. In particular, the values of displacement s_{Fmax} and s0.3Fmax are important. The larger these values are, the more energy the joint absorbs before failure, which is positive in terms of crash safety. This finding is correlated with the calculated value of the deformation work at the maximum failure force of the joint as well as with the total deformation work—Table 10. From Figure 9, it can be seen that the TL-Al flowdrill joint, although it did not exhibit the highest load-carrying capacity (Fmax = 1300 N), absorbed the most energy up to failure (W = 1.61 J). In combination with bonding, there was a significant increase in the load-carrying capacity of this joint (Fmax = 9077 N) and also an increase in energy absorption (displacement at 0.3Fmax up to 2.13 mm, WFmax = 10.31 J).

4. Discussion

This study focuses on the possibilities of joining thin-walled materials by flowdrill technology without using a screw at constant process parameters. Thus, the variables are only the material properties of the materials used and their relative position during joining.

4.1. Influence of the Position of Materials When Joining

The study showed that the position of materials with different mechanical and physical properties is important when joining them together. For given process parameters, it was

found that successful joints were always formed when one of the materials was an Al alloy. Steel-steel joints were not successful at the given parameters. This does not mean that they cannot be joined, but it does require the process parameters to be adjusted.

For successful steel-aluminum and aluminum-aluminum combinations, respectively, it has been shown that the aluminum alloy in the upper position leads to the formation of only a friction fit joint, but not an interference fit joint—there is no Al bushing formed. The aluminum alloy in the top position is only pushed out laterally, removed from the hole location, and subsequently the bushing is formed only from the steel in the lower position. Mutual interlocking is provided only by very thin steel collar. The sideways displacement of the aluminum is related to the decrease in the mechanical properties of the Al alloy at elevated temperatures.

If there is steel in the upper position, two concentric bushings will be formed and an interference fit joint will result. The Al-Al joint is partly a friction fit and partly an interference fit joint. The behavior of the materials depending on the position in the joint can be explained mainly on the basis of the physical properties of the materials.

4.2. Influence of Physical Properties of Materials on the Formation of a Joint

Ozek in [12] states that among the physical properties of materials, the thermal conductivity and melting temperature of materials are of greatest importance. The low thermal conductivity of steels compared to Al alloys (see Table 3) leads to higher frictional heat production (Streppel in [15] notes a temperature of about 600 °C for low carbon steels) and its slow dissipation from the hole surroundings. Higher thermal conductivity of Al, on the other hand, leads to faster heat dissipation to more distant material volumes and the material is heated less at the hole location. For aluminum, according to Ozek [12], a maximum hole formation temperature in the range of 240–330 °C can be expected, depending on thermal conductivity of the particular Al alloy. When joining combined materials, heating occurs mainly in the material at the upper position where the first contact with the tool occurs. If the Al sheet is in the upper position, it reaches a temperature of 330 °C, part of the temperature is dissipated by the material, part is transferred to the steel sheet. This temperature is too low for the steel sheet to soften, which then starts to plastically deform, so the tool tip that has passed through the softened aluminum starts producing heat in the steel to about 600 °C. This causes overheating of Al, a decrease in its mechanical properties near the hole, viscoplastic behavior [13], and continuous extrusion of the Al alloy sideways instead of forming a bushing. As Al is extruded laterally, a frictional joint with the steel is formed, Figure 17.
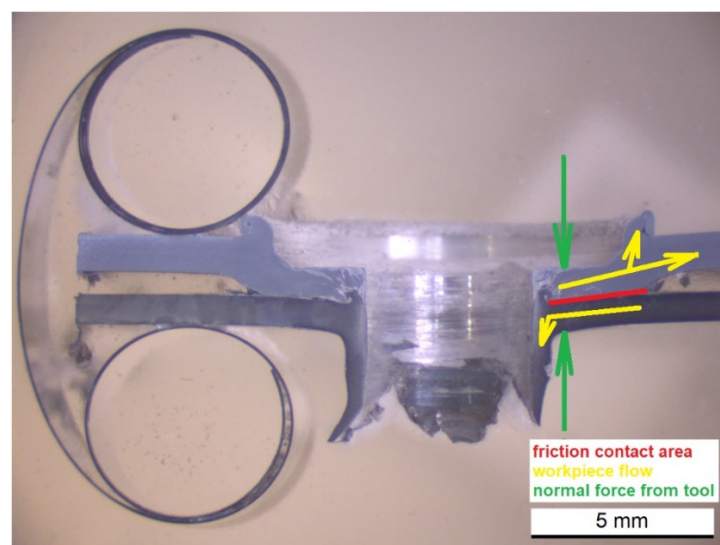

Figure 17. Scheme of friction joint formation.

However, knowing the temperature of the material at the drilling site is not sufficient. It is much more important to know the ratio of this temperature to the melting point of the material and to know the dynamics of the decrease of the mechanical properties of the workpiece with increasing temperature. For example, while a temperature of 330 °C for an EN AW 6082 T6 alloy is homologously up to $0.6 \times$ Tm, a temperature of 600 °C for a low carbon steel is only $0.4 \times$ Tm, i.e., aluminum can have a more drastic drop in mechanical properties at 300 °C than steel at 600 °C.

The situation looks different if steel is in the upper position. When the steel in the upper position is heated by frictional heat, the steel is plasticized (temperature approx. 600 °C) and is shaped by the tool, the Al alloy in the lower position is heated only by heat transfer from the steel, it will not overheat as it has a significantly higher thermal conductivity, and a continuous bushing will be formed secondarily—not as a result of shaping by the tool, but by copying the steel bushing being formed. In the process itself, contact between the tool and the aluminum may not occur at all.

4.3. Interaction of Materials When Joining

SEM analysis, Figures 7–11, did not show any material transfer in Al-DC, DC-Al joints, while in Al-TL and TL-Al combinations, the frictional heat caused the Zn layer on the TL steel plate to melt and react with Al. This results in a Zn layer uniformly deposited on the Al, and a smaller amount of Al deposited on the TL steel near the hole.

4.4. Effect of Tool Wear on Joint Formation

Under optimum conditions, the tool has a tool life of approx. 8000 holes (max. 10,000). According to [14], its surface is exposed to adverse conditions during its service life—abrasive wear, adhesive wear, oxidative wear. Insufficient heating of the material during drilling leads to sticking of microparticles of workpiece to tool surface. Too high temperatures in the drilling process lead to increased potential for oxidation on the drilling tool surface, although normally the tool surface is covered with a layer of oxides to protect the tool from sticking to the material. With time of use, the surface roughness of especially the conical part of the tool increases [12,14], which increases the frictional heat, changes the thermal conditions during drilling, and deteriorates the quality of the hole surface. Regular lubrication of the tool can slow down these changes.

5. Conclusions

This experimental study confirmed the feasibility of using flowdrill technology for joining thin-walled metallic materials. From the results obtained, the following findings can be formulated:

- Using flowdrill technology, it is possible to create an interference fit joint or friction joint, alone or in combination with adhesive bonding. As for the interference fit joint, the load-bearing capacity of the joint can be predicted based on the thickness of the inner bushing. The failure of the bushing in a form-fit joint combined with adhesive bonding can increase the absorbed energy and thus increase the safety of the joint. For friction joints, the bond strength between materials is uncertain.
- An important role in joining dissimilar materials is played by their physical properties, in particular the melting temperature and thermal conductivity of the materials. It is also useful to know the temperature dependence of the mechanical properties of the materials to be joined.
- Due to the decisive influence of the physical properties on the behavior of the materials at local heating, the position of the materials to be joined plays an important role.
- To create an interference fit joint with two concentric bushings, we recommend placing a material with a higher melting temperature in the upper position. Joints made in this way also exhibited the highest load-carrying capacity.
- Each material combination requires a search for optimum process parameters or a detailed thermal-strain modelling of the process.

- The combination of flowdrill technology with adhesive bonding results in a sealed joint, an increase in the load-bearing capacity of the joint, and a reduction in the risk of crevice or galvanic corrosion.

References

1. European Aluminium Association: Hybrid Joining Techniques. Available online: https://www.aec.org/page/extrusion-aluminum-joining-manual (accessed on 7 February 2022).
2. Messler, W.S. *Joining of Advanced Materials*, 1st ed.; Butterworth-Heinemann: Oxford, UK, 1993; 560p.
3. Sirisalee, P.; Ashby, M.F.; Parks, G.T.; John Clarkson, P. Multi-criteria material selection of monolithic and multi–materials in engineering design. *Adv. Eng. Mater.* **2006**, *8*, 48–56. [CrossRef]
4. Mori, K.; Bay, N.; Frantini, L.; Micari, F.; Tekkaya, A.E. Joining by plastic deformation. *CIRP Ann. Manuf. Technol.* **2013**, *62*, 673–694. [CrossRef]
5. Martinsen, K.; Hu, S.J.; Carlson, B.E. Joining of dissimilar materials. *CIRP Ann. Manuf. Technol.* **2015**, *64*, 679–699. [CrossRef]
6. Yang, J.; Li, Y.L.; Zhang, H. Microstructure and mechanical properties of pulsed laser welded Al/steel dissimilar joint. *Trans. Nonferrous Met. Soc. China* **2016**, *26*, 994–1002. [CrossRef]
7. Wang, B.; Sun, Z.; Xu, L.; Zhang, W.; Li, X.; Zhang, H. Friction spot joining of aluminum AA5052 and short glass fiber-reinforced PPS: Effects of material properties and process parameters on joint structure and strength. *J. Manuf. Process.* **2021**, *66*, 549–564. [CrossRef]
8. Evans, W.T.; Cox, C.; Gibson, B.T.; Strauss, A.M.; Cook, G.E. Two-sided friction stir riveting by extrusion: A process for joining dissimilar materials. *J. Manuf. Process.* **2016**, *23*, 115–121. [CrossRef]
9. Banea, M.D.; Rosioara, M.; Carbas, R.J.C.; da Silva, L.F.M. Multi-material adhesive joints for automotive industry. *Compos. B Eng.* **2018**, *151*, 71–77. [CrossRef]
10. Jeevi, G.; Nayak, S.K.; Kader, M.A. Review on adhesive joints and their application in hybrid composite structures. *J. Adhes. Sci. Technol.* **2019**, *33*, 1497–1520. [CrossRef]
11. Kleiner, M.; Geiger, M.; Klaus, A. Manufacturing of lightweight components by metal forming. *CIRP Ann. Manuf. Technol.* **2003**, *52*, 521–542. [CrossRef]
12. Haghshenas, M.; Gerlich, A.P. Joining of automotive sheet materials by friction-based welding methods: A review. *Eng. Sci. Technol. Int. J* **2018**, *21*, 130–148. [CrossRef]
13. Fang, X.; Zhang, F. Hybrid joining of a modular multi-material body-in-white structure. *J. Mater. Process. Technol.* **2020**, *275*, 116351. [CrossRef]
14. Graf, M.; Sikora, S.P.; Roider, C.S. Macroscopic modeling of thin-walled aluminium-steel connections by flow drill screws. *Thin-Walled Struct.* **2018**, *130*, 286–296. [CrossRef]
15. Shalamov, P.V.; Kulygina, I.A.; Yaroslavova, E.N. ANSYS Software-based study of thermal drilling process. *Procedia Eng.* **2016**, *150*, 746–752. [CrossRef]
16. Aslan, F.; Langlois, L.; Balan, T. Experimental analysis of the flow drill screw driving process. *Int. J. Adv. Manuf. Technol.* **2019**, *104*, 2377–2388. [CrossRef]
17. Krasauskas, P. Experimental and statistical investigation of thermo mechanical friction drilling process. *Mechanika* **2011**, *17*, 681–686. [CrossRef]
18. Miller, S.F.; Li, R.; Wang, H.; Shih, A.J. Experimental and numerical analysis of the friction drilling process. *J. Manuf. Sci. Eng.* **2006**, *128*, 802–810. [CrossRef]
19. Özek, C.; Demir, Z. Investigate the friction drilling of aluminium alloys according to the thermal conductivity. *TEM J.* **2013**, *2*, 93–101.

20.   Kumar, R.; Hynes, N.R.J. Thermal drilling processing on sheet metals: A review. *Int. J. Lightweight Mater. Manuf.* **2019**, *2*, 193–205. [CrossRef]

21.   Dehghan, S.; Ismail, M.I.S.b.; Ariffin, M.K.A.b.; Baharudin, B.T.H.T.b. Friction drilling of difficult to machine materials: Workpiece mictrostructural alterations and tool wear. *Metals* **2019**, *9*, 945. [CrossRef]

22.   Streppel, A.H.; Kals, H.J.J. Flowdrilling: A preliminary analysis of a new bush-making operation. *CIRP Ann. Manuf. Technol.* **1983**, *32*, 167–171. [CrossRef]

23.   Kumar, R.; Hynes, N.R.J.; Pruncu, C.I.; Sujana, J.A.J. Multi-objective optimization of green technology thermal drilling process using grey-fuzzy logic method. *J. Clean. Prod.* **2019**, *236*, 117711. [CrossRef]

24.   Kaya, M.T.; Aktas, A.; Beylergil, B.; Akyildiz, K.H. An experimental study on friction drilling of St12 steel. *Trans. Can. Soc. Mech. Eng.* **2014**, *38*, 319–329. [CrossRef]

25.   Kanagaraju, T.; Peter, J.S.J.; Samuel, D.R.; Prakash, J.P. Optimization of drilling parameters for thrust force and torque in friction drilling process. *Middle-East J. Sci. Res.* **2016**, *24*, 1577–1582. [CrossRef]

26.   Shalamov, P.; Pivtsaeva, M.; Chvanova, A.; Shamgunov, A. Use of combined tools to reduce axial force during thermal drilling. *Mater. Today* **2021**, *38*, 1931–1935. [CrossRef]

27.   El-Blahoul, S.A.; El-Shourbagy, H.E.; El-Blahoul, A.M.; El-Midany, T.T. Experimental and thermo-mechanical modeling optimization of thermal friction drilling for AISI 304 stainless steel. *CIRP J. Manuf. Sci. Technol.* **2018**, *20*, 84–92. [CrossRef]

28.   El-Bahloul, S.A.; El-Shourbagy, H.E.; El-Midany, T.T. Optimization of thermal friction drilling process based on taguchi method and fuzzy logic technique. *Int. J. Sci. Eng. Appl.* **2015**, *4*, 55–59. [CrossRef]

29.   Schmerler, R.; Rothe, F.; Grunert, M. Hybrid Joining Using the Flow Drill Technology. Available online: https://www.researchgate.net/publication/341616091_Hybridfugen_durch_Fliesslochformen_Hybrid_joining_using_the_flow_drill_technology (accessed on 17 January 2022).

30.   Sønstabø, J.K.; Morin, D.; Landseth, M. Testing and modelling of flow-drill screw connections under quasi-static loadings. *J. Mater. Process. Technol.* **2018**, *255*, 724–738. [CrossRef]

31.   Skovron, J.D.; Prasad, R.R.; Ulutan, D.; Mears, L.; Detwiler, D.; Paolini, D.; Baeumler, B.; Claus, L. Effect of thermal assistance on the joint quality of Al6063-T5A during flow drill screwdriving. *J. Manuf. Sci. Eng. (Trans. ASME)* **2015**, *137*, 051019. [CrossRef]

32.   *EN ISO 12996:2013*; Mechanical Joining–Destructive Testing of Joints–Specimen Dimensions and Test Procedure for Tensile Shear Testing of Single Joints. ISO: Geneva, Switzerland, 2013.